Article

Improving the HCHO Sensing Selectivity on Ag-Doped Graphene by Oxygen Functionalization: A First-Principles Study

Lunwei Yang, Wei Xiao,* Jianwei Wang,* Xiao-Wu Li, and Ligen Wang

Read Online

ACCESS | Metrics & More | Article Recommendations

ABSTRACT: Graphene-based sensors typically fail in the selectivity of target gas detection when exposed to complex and multicompound atmospheres. We have thoroughly compared the adsorptions of various interfering gases (CO, NH_3, CH_4, C_2H_2, C_2H_4, CH_3OH, and CH_3Cl) with target HCHO on AgG and AgOG by first-principles simulations. The results demonstrate that AgG shows a poor selectivity for HCHO detection and an oxygen functionalized one can improve the selectivity by enhancing the adsorption strength of HCHO and weakening those of other gas molecules. Moreover, the sensing properties of the AgOG sensors are evaluated by the NEGF method, and the predicted HCHO sensing responses are 76 and 32% along the armchair and zigzag directions, respectively. The present work helps shed some light on designing graphene-based sensing materials with high selectivity.
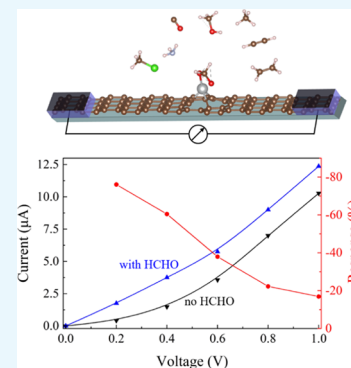
1. INTRODUCTION

As a simple organic aldehyde molecule, formaldehyde is one of the important chemical products in glues, adhesives, paper making, clothing, and rubber industry production, with an annual output of over 46 billion pounds.[1] In a long period, indoor formaldehyde is slowly and continuously released from the above sources, which is highly irritating, toxic, and carcinogenic and seriously endangers environmental safety and human health.[2,3] Formaldehyde has been identified as a major contributor to the sick-building syndrome, which is typically characterized by dizziness, headache, eye and throat irritations, chest tightness, and more severe infertility, deformity, and cancer.[4,5] Gas sensing technology that can detect formaldehyde in real-time and conveniently is particularly beneficial for our life.

Nowadays, graphene-based materials have attracted tremendous interest and attention in the field of gas sensors due to their high surface area ratio, carrier mobility, and electrical conductivity.[6,7] Recent experiments report that Ag-decorated graphene has been successfully prepared by different methods, such as thermal exfoliation under protective gas[8] and wet-spinning combined chemical reduction.[9] In our previous calculations, we have systematically investigated the HCHO adsorption and sensing properties of graphene sheet doped with more than 13 transition metals (TMs). By comparing the adsorption and sensing performance with Ag or with other TM, we found that Ag-doped graphene is one of the most potential candidates for HCHO sensing application with a short response time and high sensitivity.[10] However, sensing selectivity, which refers to the characteristics that determine

whether a sensor can respond to a specific molecule, is another key parameter for an excellent sensor.[11] The formaldehyde detection environment is extremely complex and always coexists with a variety of volatile organic chemicals and common gas pollutants.[12] Coexisting gases may affect the adsorption and sensing process of the target formaldehyde molecule on the surface of the sensing materials, and poor selectivity could hinder the practical application of formaldehyde sensors.

Conventional chemical modification of graphene might provide a variety of possibilities for regulating its chemical and physical properties.[13] Oxygen plasma treatment is a widely used, controllable, and effective experimental method for regulating the surfaces, carrier densities, and electronic structures of graphene-base materials, which could significantly improve the sensitivity and selectivity.[14−17] In this paper, the HCHO selective adsorption for the Ag-doped graphene (AgG) and the oxygen plasma-treated AgG (AgOG) has been thoroughly investigated in the framework of the density functional theory. Various interfering gases (CO, NH_3, CH_4, C_2H_2, C_2H_4, CH_3OH, and CH_3Cl) on their surfaces have been involved in the simulations. The calculations demonstrate that the adsorption of several molecules on the AgG surface is
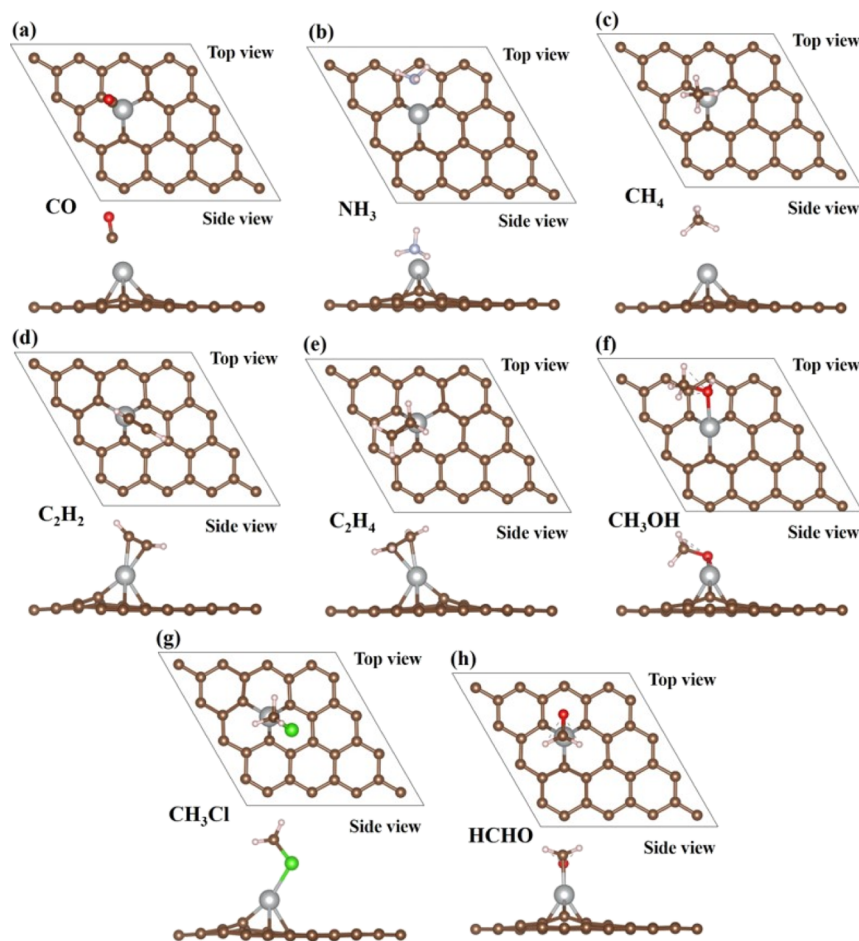
Figure 1. (Color online) Top and side views of the most favorable configurations for (a−h) CO, NH_3, CH_4, C_2H_2, C_2H_4, CH_3OH, CH_3Cl, and HCHO molecules on the AgG substrate, respectively. The brown, silver, gray, red, green, and white balls indicate C, Ag, N, O, Cl, and H atoms, respectively.

stronger than formaldehyde, which suggests a poor selectivity for the sensing of formaldehyde, and oxygen functionalization can overcome the challenge of the poor selectivity. After the oxygen functionalization of the AgG surface, the adsorption strength of these interfering gases is significantly decreased, but that of formaldehyde is increased. Moreover, the two-probe AgOG nano-sensor for HCHO detecting is built to simulate its sensing properties. The results show that the AgOG could have large enough HCHO sensing responses of 76 and 32% in the armchair and zigzag directions, respectively.

2. COMPUTATION AND METHOD DETAILS

The Vienna ab initio simulation package code,[18,19] is employed to solve the Kohn−Sham equations in the projector-augmented wave basis set in this paper. The PBE exchange−correlation functional[20] is used, which is based on the generalized gradient approximation. The valence electron configurations in the states of 1s for H, 2s 2p for C, N, and O, 3s 3p for Cl, and 4d 5s for Ag are chosen. The plane-wave basis set with a kinetic energy cutoff of 500 eV is employed. The geometry optimizations are performed using the conjugate gradient algorithm until the self-consistent energy convergence threshold and the Hellman−Feynman forces are smaller than 10^{-5} eV and 0.01 eV/Å, respectively. A semiempirical Grimme's DFT-D2[21] correction is employed to describe the van der Waals interaction in the optimizations and electronic

structure calculations. The monolayer graphene sheet is modeled with a (4×4) unit cell and a vacuum spacing of 15 Å is added to avoid the interaction between adjacent periodic cells. The reciprocal space of the graphene sheet is sampled with a $(5 \times 5 \times 1)$ and $(15 \times 15 \times 1)$ k-point grid automatically generated by the Monkhorst−Pack method[22] for atomic relaxations and electronic structure simulations, respectively. The optimized lattice constant of graphene is 2.45 Å, which is in good agreement with the experimental value.[23]

The charge transfers Δq based on the Bader charge analysis[24] are calculated to analyze the interaction mechanisms of gas molecules absorbed systems. A positive Δq indicates that electrons transfer from the graphene substrate to gas molecules, and vice versa. The adsorption energy of gas molecules on the substrate is calculated through the correction of zero-point energy (ZPE)[25] of gas molecules by using the following equation

$$\Delta E_{ads} = E_{tot} - E_{sub} - E_{mol} + \Delta E_{ZPE} \qquad (1)$$

where E_{tot}, E_{sub}, and E_{mol} represent the total energies of the relaxed gas molecule on the substrate, the substrate and the isolated gas molecule, respectively. ΔE_{ZPE} is the ZPE change of gas molecules between adsorbing upon the substrate and the free phase. A negative value of ΔE_{ads} corresponds to a stable adsorption structure.

Table 1. Summary for Various Gas Absorbates Adsorbed on the AgG Substrate[a]

absorbates	CO	NH$_3$	CH$_4$	C$_2$H$_2$	C$_2$H$_4$	CH$_3$OH	CH$_3$Cl	HCHO
d/Å	2.01	2.22	2.57	2.18	2.23	2.28	2.51	2.14
Δq/e	0.11	−0.16	−0.02	0.07	0.02	−0.07	−0.09	0.29
ΔE_{ZPE}/eV	0.05	0.11	0.01	0.02	0.06	0.07	0.03	0.06
ΔE_{ads}/eV	−1.10	−1.08	−0.20	−1.07	−1.17	−0.89	−0.52	−0.88

[a]The shortest distance between the Ag dopant and the gas molecule, the Bader charge gain Δq of various gas molecules from the substrate, the ZPE correction of gas molecules before and upon adsorption, and the gas adsorption energy with the ZPE correction are presented.
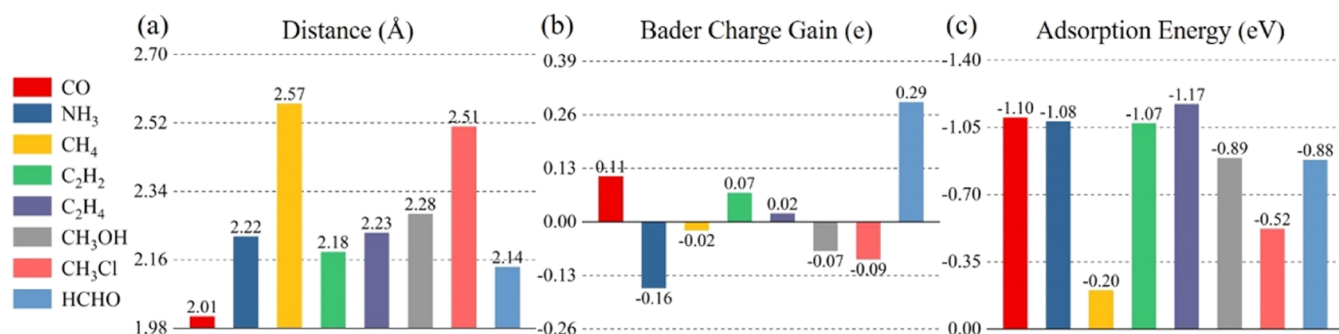

Figure 2. (Color online) (a) Shortest adsorption distance between the AgG substrate and the absorbates, (b) the Bader charge gain Δq of various gas molecules from the substrate, and (c) the adsorption energy of various gas molecules adsorbed on the AgG substrate.
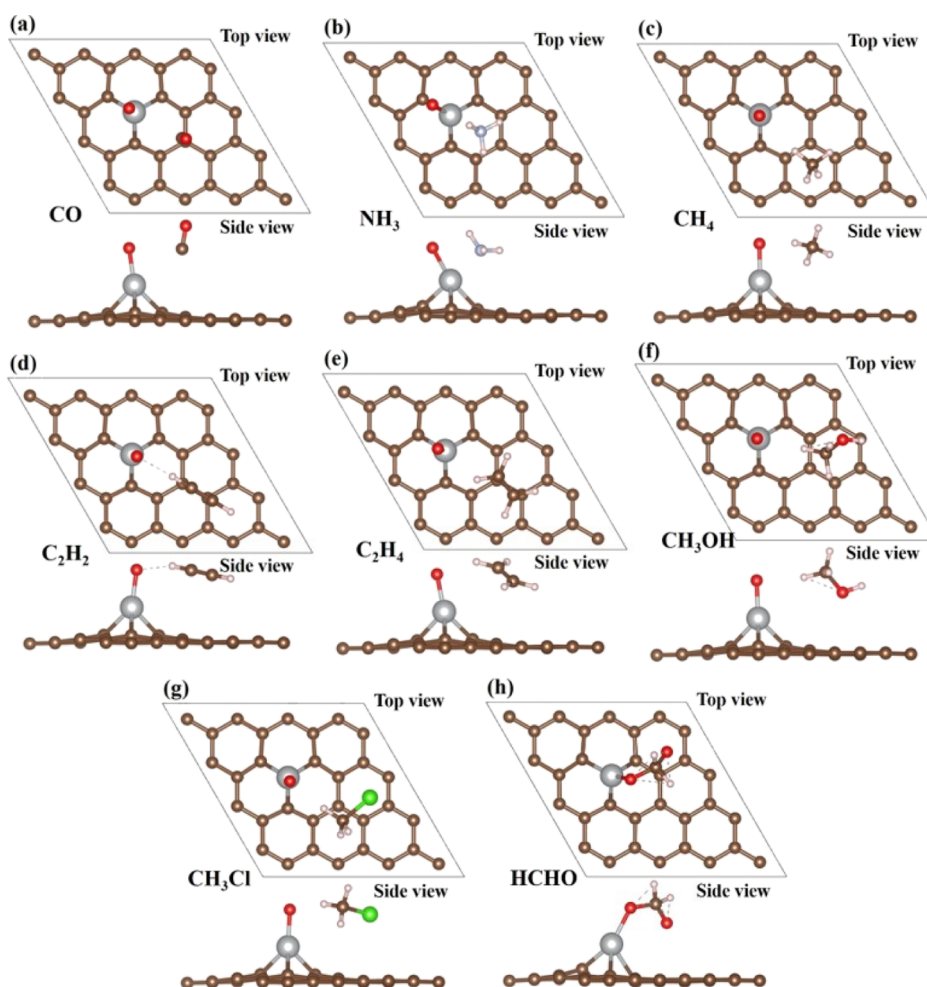

Figure 3. (Color online) Top and side views of the most favorable configurations for (a−h) CO, NH$_3$, CH$_4$, C$_2$H$_2$, C$_2$H$_4$, CH$_3$OH, CH$_3$Cl, and HCHO molecules on the AgOG substrate, respectively. The brown, silver, gray, red, green, and white balls indicate C, Ag, N, O, Cl, and H atoms, respectively.

Table 2. Summary for Various Gas Absorbates Adsorbed on the AgOG Substrate[a]

absorbates	CO	NH$_3$	CH$_4$	C$_2$H$_2$	C$_2$H$_4$	CH$_3$OH	CH$_3$Cl	HCHO
d/Å	2.99	2.24	2.28	2.10	2.25	2.36	2.16	1.39
Δq/e	0.017	−0.178	0.005	0.011	−0.005	0.004	0.002	−0.341
ΔE_{ZPE}/eV	0.02	0.10	0.03	0.02	0.03	0.03	0.02	0.03
ΔE_{ads}/eV	−0.15	−0.61	−0.17	−0.35	−0.23	−0.33	−0.34	−1.16

[a]The shortest distance between the Ag dopant and the gas molecule, the Bader charge gain Δq of various gas molecules from the substrate, the ZPE correction of gas molecules before and upon adsorption, and the gas adsorption energy with the ZPE correction are listed.
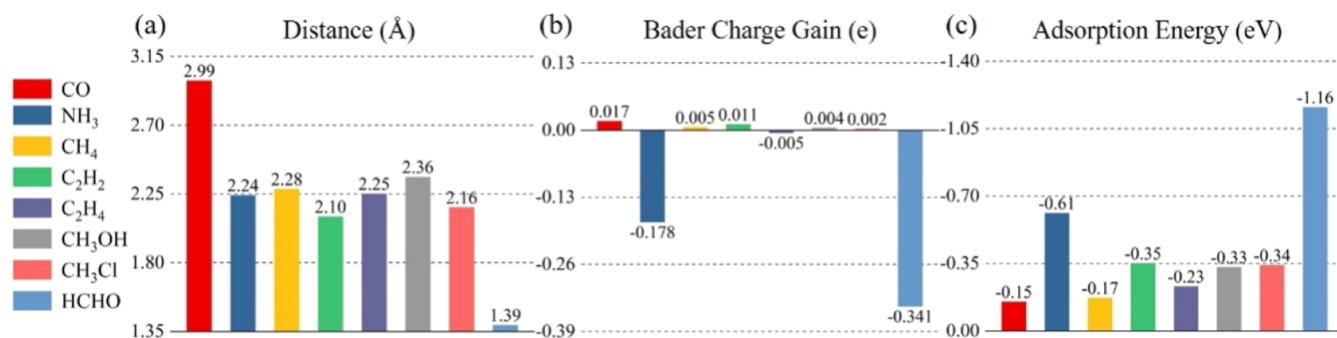

Figure 4. (Color online) (a) Shortest adsorption distance between the AgOG substrate and the absorbates, (b) the Bader charge gain Δq of various gas molecules from the substrate, and (c) the adsorption energy of various gas molecules adsorbed on the AgOG substrate.

The sensing properties have been evaluated using the Nanodcal package which combines the DFT method with nonequilibrium Green's function (NEGF).[26,27] The basis set is adopted with a double-ζ plus polarization and the energy cutoff of the real-space grid is taken as 100 Ha. The current flow through the transport model is defined by the Landauer−Büttiker formula[28]

$$I = G_0 \int_{\mu_R}^{\mu_L} T(E, V_b)dE \qquad (2)$$

in which G_0 is the quantum conductance unit. $T(E,V_b)$ is the transmission coefficient. $\mu_{L/R}$ is the chemical potential of the left or right electrode. V_b is the bias voltage defined as the electrochemical potential difference between the left and right electrodes.

3. RESULTS AND DISCUSSION

3.1. Gas Adsorption on the AgG Substrate. The AgG structure can be obtained by replacing one carbon atom with an Ag atom. The surface composition of Ag in the doped graphene is about 3 at %, and the parameter of the relaxed AgG structure ($d_{Ag−C}$ = 2.20 Å, h_{Ag} = 1.90 Å) is consistent with previous research studies.[29,30] Before the study of the adsorption processes, all interfering gases (CO, NH$_3$, CH$_4$, C$_2$H$_2$, C$_2$H$_4$, CH$_3$OH, and CH$_3$Cl) and target HCHO are fully relaxed, and their geometry parameters are corresponding well with the results listed in the CRC handbook.[31] The Ag dopant can cause the local bending of the graphene surface and always plays as an active site to adsorb gas molecules. Therefore, the gas molecule is placed around the Ag dopant in relatively different positions and orientations to build initial adsorption models. Figure 1 shows the most stable adsorption geometries of different gases adsorbed on the AgG substrate. Their corresponding shortest distance between the dopant atom and the gas molecule, the Bader charge gain Δq of HCHO molecule from the substrate, the ZPE correction of difference gas adsorbates before and upon adsorption, and the adsorbate

adsorption energy with the ZPE correction are all summarized in Table 1 and presented in Figure 2.

From Table 1 and Figure 2, the adsorption characteristics of interfering gases and target HCHO absorbed onto the AgG can be compared. At first, we can see that some molecules, such as CO, NH$_3$, C$_2$H$_2$, C$_2$H$_4$, and CH$_3$OH have higher adsorption energies ranging from −0.89 to −1.17 eV with shorter adsorption distances between 2.01 and 2.28 Å. CH$_4$ and CH$_3$Cl have lower adsorption energies (−0.20 and −0.52 eV) with larger adsorption distances of 2.57 and 2.51 Å, respectively. Those molecules (CO, NH$_3$, C$_2$H$_2$, C$_2$H$_4$, and CH$_3$OH) having stronger interaction than HCHO could preferentially occupy the activity sites of the AgG and directly interfere with the adsorption behavior and sensing performance of the target gas, which could be detrimental to the properties of the sensing materials. The charge transfer results of gas adsorbates in Figure 2 demonstrate that CO, C$_2$H$_2$, C$_2$H$_4$, and HCHO act as charge acceptors which gain electrons from the AgG substrate, while NH$_3$, CH$_4$, CH$_3$OH, and CH$_3$Cl are charge donors. Among all gas molecules, the amount of transfer charge between the HCHO molecule and the AgG substrate is the largest (0.29 e), which is consistent with the reported large sensing response to formaldehyde.[10] In general, due to the interference of other gases, the AgG substrate might miss in selective adsorption for the target HCHO molecule and the accuracy and precision of the gas sensor could be seriously impeded.

3.2. Gas Adsorption on the AgOG. For the optimized AgOG systems, the Ag−O bond is 1.83 Å and the Ag−C bond is slightly compressed by an average of 0.09 Å. A similar geometric structure of the Si-doped graphene functionalized with oxygen was also employed in the previous paper.[32] The gas absorbates adsorbed on the AgOG substrate have also been thoroughly investigated. The final stable adsorption geometries of various gases adsorbed on the AgOG substrate are shown in Figure 3, and the related properties for these gases after adsorption are summarized in Table 2 and also presented in Figure 4.

Compared with the AgG substrate, the adsorption behaviors of these gas molecules on the AgOG substrate have been dramatically changed. For the adsorption of CO, CH_4, C_2H_2, C_2H_4, CH_3OH, and CH_3Cl, the geometries of the molecules remain essentially unchanged. Their adsorption energies are in the range from -0.15 to -0.35 eV, and their charge transfers are between -0.05 and 0.17 e. Weak adsorption strength combined with small charges transfer indicates that CO, CH_4, C_2H_2, C_2H_4, CH_3OH, and CH_3Cl are physisorbed upon the AgOG substrate. As for NH_3, its adsorption energy is also reduced to -0.61 eV, but higher than other interfering gases mentioned above. However, when bonded to the AgOG substrate, the HCHO molecule forms a C—O bond of 1.39 Å as shown in Figure 3h. A strong C—O bond means that it is difficult for the HCHO molecule to desorb from the AgOG substrate, thus affecting its recovery time and working temperature. In experiments, pretreatment methods such as heating or ultraviolet radiation are often used to accelerate the recovery of sensors.[33] The charge transfer results demonstrate that the HCHO molecule changes from the largest electron acceptor (0.29 e) on the AgG substrate to the largest electron donor (-0.341 e) on the AgOG substrate. The change of the bonding environment makes the adsorption energy of HCHO upon the AgOG substrate increase to -1.16 eV, which can also be verified by the shortest adsorption distance. The medium adsorption strength (-0.80 to -1.2 eV) could be more conducive to the desorption of the measured gas on the sensor, which is favorable for reducing the recovery time in industrial application.[10,34] With the lowest adsorption energy, the target HCHO could be most easily and selectively adsorbed to the AgOG substrate. Moreover, with a larger amount of charge transfer in the adsorption process, it may be expected that the sensing response of the HCHO molecules on the AgOG sensing material would be the highest.

3.3. Electronic Structures. We choose C_2H_4 and HCHO molecules to study the interaction in the process of adsorption. The charge density difference maps between the molecules and the AgG or AgOG substrate are plotted to quantitatively analyze the electron distribution, which is defined as $\Delta\rho = \rho_{tot} - \rho_{sub} - \rho_{mol}$. Here, ρ_{tot}, ρ_{sub}, and ρ_{mol} denote the charge densities of the gas molecule absorbed on the substrate, the substrate and the isolated gas molecule, respectively. There is significant electron gain or loss in the region between the AgG or AgO substrate and the C_2H_4 or HCHO adsorbate from Figure 5a,b,d, which imply strong orbital hybridization during the adsorption. For C_2H_4 adsorption on the AgOG substrate in Figure 5c, the electron interaction is rare, which confirms the

weak physisorption between the molecule and the substrate. Also, we can see the yellow iso-surface in Figure 5a,b are mainly distributed around C_2H_4 and HCHO adsorbates, demonstrating that the gas molecules gain electrons from the AgG substrate, which is consistent with the results of the Bader charge analysis above. Interestingly, it is expected that the introduction of an oxygen atom makes the substrate turn to be an electron acceptor from an electron donor. Based on our previous study,[10] the change induced by HCHO adsorption could increase the conductivity of the AgOG substrate.

Furthermore, the densities of states (DOSs) have also been plotted in Figure 6 to understand the underlying orbital interactions between the AgG or AgOG substrate and the C_2H_4 or HCHO molecule. From Figure 6c,d, we can find that the electron states of these molecules are distributed throughout the entire energy scope, even with some electron states across the Fermi level. It means that there is strong orbital hybridization between the C_2H_4 or HCHO molecule and the Ag dopant, and thus, the C_2H_4 or HCHO molecule can tightly bind to the AgG substrate. However, it is found in Figure 6e that the electron states of C_2H_4 after adsorption on the AgOG substrate turn to be some discontinuous isolated peaks, similar to the free molecule in Figure 6a. By comparing the DOSs in Figure 6d,f, it can be expected that the orbitals of the HCHO molecule hybrid more strongly with the Ag—O group on the AgOG substrate than with the Ag on the AgG substrate, proving that the adsorption of HCHO upon the AgOG substrate is enhanced. Moreover, the higher peak at the Fermi level when HCHO adsorbing on the AgOG substrate indicates that HCHO adsorption might affect the conductivity of the AgOG substrate.

3.4. Sensing Properties. In the framework of the NEGF-DFT method, the electronic sensing properties of the AgOG substrate for HCHO detecting are simulated by NanoDcal code. Two-probe AgOG nano-sensors with or without HCHO adsorption are built as transport models. Considering the anisotropy of the graphene lattice, the schematic structures of the gas sensors with two transport directions, that is, armchair and zigzag directions, are given in Figure 7. The nano-sensors are composed of three parts, namely, the left and right semi-infinite perfect graphene electrodes and the central AgOG scattering region without or with HCHO adsorption.

Sensing response is one of the key parameters for gas sensing device in practical applications, and it is defined with $S = [(R - R_0)/R_0] = [(I_0 - I)/I] \times 100\%$, in which R_0 or I_0 is the initial electrical resistance or current of the sensor and R or I is the measured resistance or current for the target gas under different bias voltages. According to the eq 2, we obtain the current–voltage (I–V) curves and the corresponding sensing responses of the nano-sensor to the HCHO molecule, as shown in Figure 8. The differences of I–V characteristics along the armchair-direction and zigzag-directions verify the transport anisotropy of graphene-base devices.[35,36] For both transport directions, the current through the AgOG nano-sensor increases significantly after HCHO adsorption. In our previous work,[10] it is found that HCHO adsorption could decrease the conductance on the AgG substrate. The opposite phenomenon can be explained by the electronic interactions that the HCHO molecule changes from an electron acceptor adsorbed on the AgG substrate to an electron donor upon the AgOG substrate. The maximum absolute responses of the AgOG nano-sensors to the HCHO molecule are 76 and 32% for the armchair and zigzag directions, respectively. Also, we
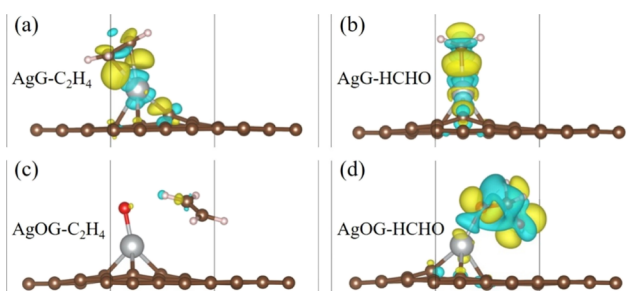

Figure 5. (Color online) Charge density difference maps for C_2H_4 and HCHO on the AgG (a,b), and AgOG (c,d) substrates. The cyan or yellow iso-surface (0.003 e/Å³ iso-surface level) represents electron accumulation or depletion.
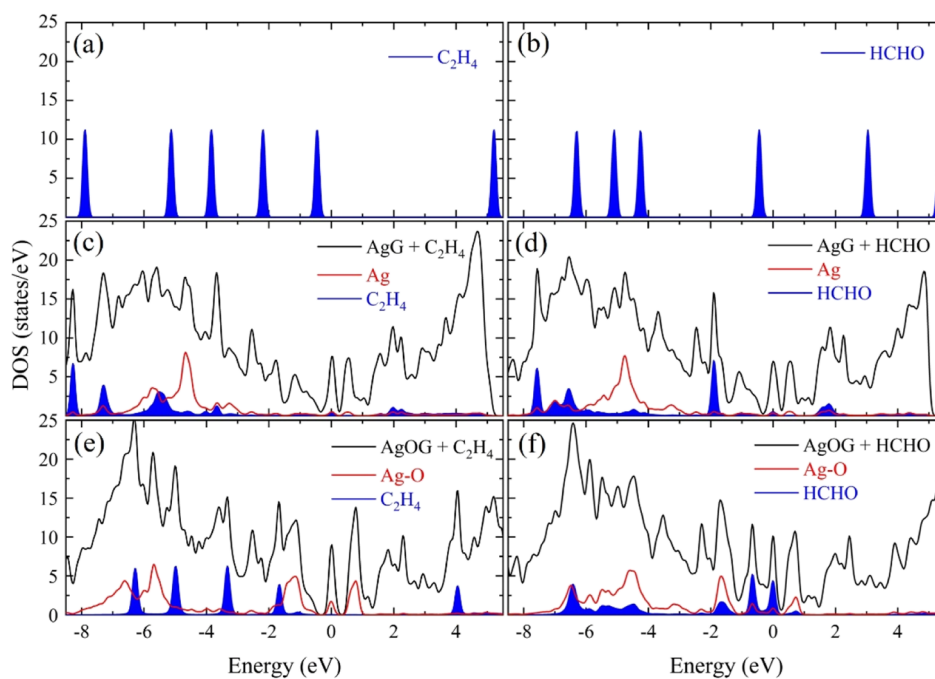
Figure 6. (Color online) (a,b) Total DOSs of free C_2H_4 and HCHO, and (c−f) total DOSs of the AgG substrate and AgOG substrate with C_2H_4 and HCHO molecule adsorption (black lines) and the projected DOSs of the Ag atom or Ag−O group (red lines) and adsorbed gas molecule (blue regions). The Fermi level is shifted to zero.
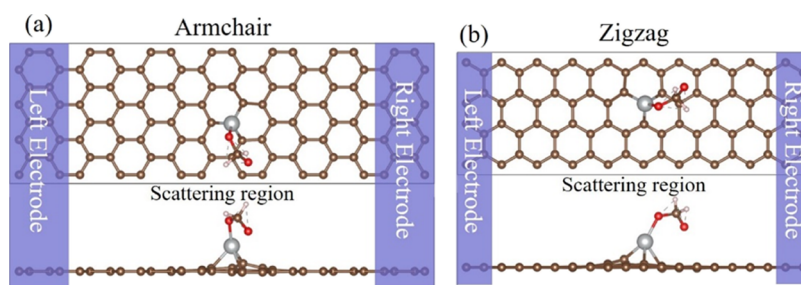

Figure 7. (Color online) Illustration of the two-probe AgOG nano-sensors to HCHO molecule where semi-infinite left and right perfect graphene electrode regions (purple shade zone) are in contact with the scattering region. Top and side views along the armchair (a) and zigzag (b) directions are depicted. The brown, gray, red, and white balls indicate C, Ag, O, and H atoms, respectively.
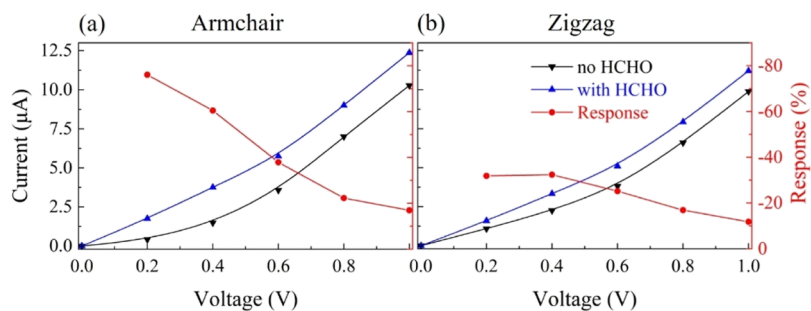

Figure 8. (Color online) Current−voltage curves and sensing responses along the armchair (a) and zigzag (b) directions for the AgOG nano-sensors without and with HCHO adsorption under the bias voltage from 0 to 1.0 V.

can observe that when the bias voltage is increased to 1 V, the absolute sensing responses along the armchair and zigzag directions gradually decrease to 16 and 11%, respectively. Furthermore, the average absolute responses of the device are calculated to be 43 and 24%, respectively, which can be considered to have sufficient sensitivity for HCHO molecule detecting.

The transmission spectra under various bias voltages are plotted in Figure 9 to analyze the sensing mechanisms of the AgOG nano-sensors to the HCHO molecule. The value of current within the bias window can be evaluated by the integration of the transmission coefficients according to eq 2, and thus, the larger the transmission area, the greater the current flowing through the device. Obviously, the HCHO
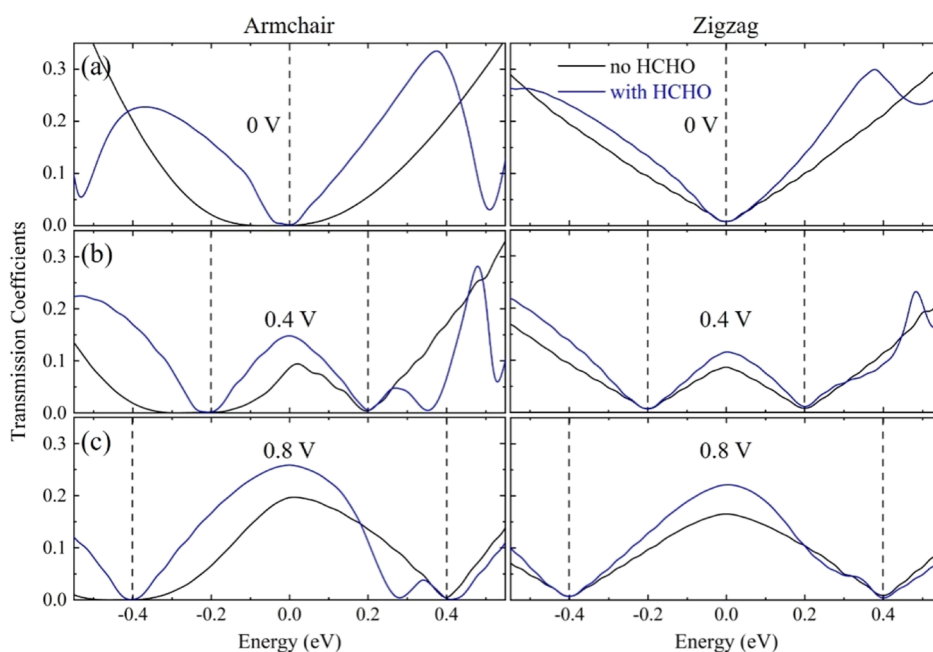
Figure 9. (Color online) Transmission spectra for the AgOG sensor adsorbed without and with the HCHO molecule along the armchair and zigzag directions under the bias voltages (a–c) 0, 0.4, and 0.8 V. The dashed lines indicate the bias voltage windows, and the Fermi energy is shifted to zero.

molecule adsorption significantly affects the transmission spectra for the AgOG sensors along both the armchair and zigzag directions. Under zero bias, the transmission coefficient of the nano-sensors without HCHO adsorption for both armchair and zigzag directions is zero, and with HCHO adsorption, the transmission spectra around the Fermi level for the armchair direction become remarkably larger than the zigzag direction. As the bias increases, the transmission spectra for both transport directions move to a wider scope, and the corresponding transmission area gradually increases. The transmission spectrum area of the nano-sensor with HCHO adsorption is always larger than that without HCHO adsorption, which could fairly support the proposed deduction that the conductivity of the AgOG substrate increases after HCHO adsorption. Because the transmission spectrum difference of the nano-sensor under various bias voltages before and after HCHO adsorption for the armchair direction is larger than that of the zigzag direction, the AgOG nano-sensor having the armchair structure is supposed to have a larger sensing response. Thus, the sensing mechanism of the AgOG nano-sensors to the HCHO molecule can be well understood.

4. CONCLUSIONS

In this paper, we have discussed the HCHO selective adsorption on the AgG and oxygen plasma-treated AgG substrates with other gases, such as CO, NH_3, CH_4, C_2H_2, C_2H_4, CH_3OH, and CH_3Cl by using first-principles calculations. Their stable adsorption geometries and energies have been studied and the results show that the AgG is more susceptible to the interference of other gases, and oxygen functionalization can overcome the challenge of poor selectivity. Upon the AgOG, not only the adsorption of interfering gases has been largely weakened but also the HCHO turn to be more preferential to be adsorbed on the substrate. Furthermore, the sensing properties of the AgOG

sensor have been evaluated by the NEGF-DFT method, and it shows that the AgOG could have large enough HCHO sensing responses of 76 and 32% in the armchair and zigzag directions, respectively. This work demonstrates that the oxygen plasma-treated AgG substrate could extremely improve the selective adsorption of HCHO molecules from various interfering gases and make it desirable to be a candidate for future sensing materials.

■ AUTHOR INFORMATION

Corresponding Authors

Wei Xiao − *State Key Laboratory of Nonferrous Metals and Processes, GRIMN Group Co., Ltd., Beijing 101417, P. R. China; GRIMAT Engineering Institute Co., Ltd., Beijing 100088, P. R. China; General Research Institute for Nonferrous Metals, Beijing 100088, P. R. China;* orcid.org/0000-0001-9447-3279; Email: xiaowei@grinm.com

Jianwei Wang − *State Key Laboratory of Nonferrous Metals and Processes, GRIMN Group Co., Ltd., Beijing 101417, P. R. China; GRIMAT Engineering Institute Co., Ltd., Beijing 100088, P. R. China; General Research Institute for Nonferrous Metals, Beijing 100088, P. R. China;* Email: wangjianwei@grinm.com

Authors

Lunwei Yang − *State Key Laboratory of Nonferrous Metals and Processes, GRIMN Group Co., Ltd., Beijing 101417, P. R. China; GRIMAT Engineering Institute Co., Ltd., Beijing 100088, P. R. China; General Research Institute for Nonferrous Metals, Beijing 100088, P. R. China; Department of Materials Physics and Chemistry, School of Materials Science and Engineering, Key Laboratory for Anisotropy and Texture of Materials, Ministry of Education, Northeastern University, Shenyang 110819, P. R. China;* orcid.org/0000-0001-7489-6215

Xiao-Wu Li − *Department of Materials Physics and Chemistry, School of Materials Science and Engineering, Key Laboratory for Anisotropy and Texture of Materials, Ministry of Education, Northeastern University, Shenyang 110819, P. R. China;* ● orcid.org/0000-0002-0238-9107

Ligen Wang − *State Key Laboratory of Nonferrous Metals and Processes, GRIMN Group Co., Ltd., Beijing 101417, P. R. China; GRIMAT Engineering Institute Co., Ltd., Beijing 100088, P. R. China; General Research Institute for Nonferrous Metals, Beijing 100088, P. R. China*

Complete contact information is available at:
https://pubs.acs.org/10.1021/acsomega.2c01383

Notes

The authors declare no competing financial interest.

■ REFERENCES

(1) Zhang, L.; Steinmaus, C.; Eastmond, D. A.; Xin, X. K.; Smith, M. T. Formaldehyde exposure and leukemia: a new meta-analysis and potential mechanisms. *Mutat. Res., Rev. Mutat. Res.* **2009**, *681*, 150−168.

(2) Cockcroft, D. W.; Hoeppner, V. H.; Dolovtch, J. Occupational asthma caused by cedar urea formaldehyde particle board. *Chest* **1982**, *82*, 49−53.

(3) Tang, X.; Bai, Y.; Duong, A.; Smith, M. T.; Li, L.; Zhang, L. Formaldehyde in China: production, consumption, exposure levels, and health effects. *Environ. Int.* **2009**, *35*, 1210−1224.

(4) Korpan, Y. I.; Gonchar, M. V.; Sibirny, A. A.; Martelet, C.; El'skaya, A. V.; Gibson, T. D.; Soldatkin, A. P. Development of highly selective and stable potentiometric sensors for formaldehyde determination. *Biosens. Bioelectron.* **2000**, *15*, 77−83.

(5) Dou, K.; Chen, G.; Yu, F.; Liu, Y.; Chen, L.; Cao, Z.; Chen, T.; Li, Y.; You, J. Bright and sensitive ratiometric fluorescent probe enabling endogenous FA imaging and mechanistic exploration of indirect oxidative damage due to FA in various living systems. *Chem. Sci.* **2017**, *8*, 7851−7861.

(6) Yoo, E.; Kim, J.; Hosono, E.; Zhou, H.-s.; Kudo, T.; Honma, I. Large reversible Li storage of graphene nanosheet families for use in rechargeable lithium ion batteries. *Nano Lett.* **2008**, *8*, 2277−2282.

(7) Zhang, B.; Cui, T. An ultrasensitive and low-cost graphene sensor based on layer-by-layer nano self-assembly. *Appl. Phys. Lett.* **2011**, *98*, 073116.

(8) Giovanni, M.; Poh, H. L.; Ambrosi, A.; Zhao, G.; Sofer, Z.; Šaněk, F.; Khezri, B.; Webster, R. D.; Pumera, M. Noble metal (Pd, Ru, Rh, Pt, Au, Ag) doped graphene hybrids for electrocatalysis. *Nanoscale* **2012**, *4*, 5002−5008.

(9) Xu, Z.; Liu, Z.; Sun, H.; Gao, C. Highly electrically conductive Ag-doped graphene fibers as stretchable conductors. *Adv. Mater.* **2013**, *25*, 3249−3253.

(10) Yang, L.; Xiao, W.; Wang, J.; Li, X.; Wang, L. Formaldehyde gas sensing properties of transition metal-doped graphene: a first-principles study. *J. Mater. Sci.* **2021**, *56*, 12256−12269.

(11) Smulko, J. M.; Trawka, M.; Granqvist, C. G.; Ionescu, R.; Annanouch, F.; Llobet, E.; Kish, L. B. New approaches for improving selectivity and sensitivity of resistive gas sensors: a review. *Sens. Rev.* **2015**, *35*, 340−347.

(12) Salthammer, T.; Mentese, S.; Marutzky, R. Formaldehyde in the indoor environment. *Chem. Rev.* **2010**, *110*, 2536−2572.

(13) Liu, J.; Tang, J.; Gooding, J. J. Strategies for chemical modification of graphene and applications of chemically modified graphene. *J. Mater. Chem.* **2012**, *22*, 12435−12452.

(14) Nourbakhsh, A.; Cantoro, M.; Vosch, T.; Pourtois, G.; Clemente, F.; van der Veen, M. H.; Heyns, M. M.; De Gendt, S.; Sels, B. F.; Sels, B. F. Bandgap opening in oxygen plasma-treated graphene. *Nanotechnology* **2010**, *21*, 435203.

(15) Mao, H.; Wang, R.; Zhong, J.; Zhong, S.; Chen, W. Mildly O2 plasma treated CVD graphene as a promising platform for molecular sensing. *Carbon* **2014**, *76*, 212−219.

(16) Wu, H.; Bu, X.; Deng, M.; Chen, G.; Zhang, G.; Li, X.; Wang, X.; Liu, W. A Gas Sensing Channel Composited with Pristine and Oxygen Plasma-Treated Graphene. *Sensors* **2019**, *19*, 625.

(17) Li, H.; Singh, A.; Bayram, F.; Childress, A. S.; Rao, A. M.; Koley, G. Impact of oxygen plasma treatment on carrier transport and molecular adsorption in graphene. *Nanoscale* **2019**, *11*, 11145−11151.

(18) Kresse, G.; Furthmüller, J. Efficient iterative schemes for ab initio total-energy calculations using a plane-wave basis set. *Phys. Rev. B: Condens. Matter Mater. Phys.* **1996**, *54*, 11169.

(19) Kresse, G.; Joubert, D. From ultrasoft pseudopotentials to the projector augmented-wave method. *Phys. Rev. B: Condens. Matter Mater. Phys.* **1999**, *59*, 1758−1775.

(20) Perdew, J. P.; Burke, K.; Ernzerhof, M. Generalized gradient approximation made simple. *Phys. Rev. Lett.* **1996**, *77*, 3865.

(21) Grimme, S. Semiempirical GGA-type density functional constructed with a long-range dispersion correction. *J. Comput. Chem.* **2006**, *27*, 1787−1799.

(22) Monkhorst, H. J.; Pack, J. D. Special points for Brillouin-zone integrations. *Phys. Rev. B: Solid State* **1976**, *13*, 5188−5192.

(23) N'Diaye, A. T.; Plasa, T. N.; Busse, C.; Michely, T. Structure of epitaxial graphene on Ir (111). *New J. Phys.* **2008**, *10*, 043033.

(24) Henkelman, G.; Arnaldsson, A.; Jónsson, H. A fast and robust algorithm for Bader decomposition of charge density. *Comput. Mater. Sci.* **2006**, *36*, 354−360.

(25) Govender, A.; Ferre, D. C.; Niemantsverdriet, J. W. H. A density functional theory study on the effect of zero-point energy corrections on the methanation profile on Fe(100). *ChemPhysChem* **2012**, *13*, 1591−1596.

(26) Taylor, J.; Guo, H.; Wang, J. Ab initio modeling of quantum transport properties of molecular electronic devices. *Phys. Rev. B: Condens. Matter Mater. Phys.* **2001**, *63*, 245407.

(27) Brandbyge, M.; Mozos, J.-L.; Ordejón, P.; Taylor, J.; Stokbro, K. Density-functional method for nonequilibrium electron transport. *Phys. Rev. B: Condens. Matter Mater. Phys.* **2002**, *65*, 165401.

(28) Büttiker, M.; Imry, Y.; Landauer, R.; Pinhas, S. Generalized many-channel conductance formula with application to small rings. *Phys. Rev. B: Condens. Matter Mater. Phys.* **1985**, *31*, 6207−6215.

(29) Krasheninnikov, A. V.; Lehtinen, P. O.; Foster, A. S.; Pyykkö, P.; Nieminen, R. M. Embedding transition-metal atoms in graphene: structure, bonding, and magnetism. *Phys. Rev. Lett.* **2009**, *102*, 126807.

(30) Düzenli, D. A Comparative Density Functional Study of Hydrogen Peroxide Adsorption and Activation on the Graphene Surface Doped with N, B, S, Pd, Pt, Au, Ag, and Cu Atoms. *J. Phys. Chem. C* **2016**, *120*, 20149−20157.

(31) Haynes, W. M. *CRC Handbook of Chemistry and Physics*; CRC Press, 2014.

(32) Lv, R.; dos Santos, M. C.; Antonelli, C.; Feng, S.; Fujisawa, K.; Berkdemir, A.; Cruz-Silva, R.; Elías, A. L.; Perea-Lopez, N.; López-Urías, F.; Terrones, H.; Terrones, M. Large-area Si-doped graphene: controllable synthesis and enhanced molecular sensing. *Adv. Mater.* **2014**, *26*, 7593−7599.

(33) Li, J.; Lu, Y.; Ye, Q.; Cinke, M.; Han, J.; Meyyappan, M. Carbon Nanotube Sensors for Gas and Organic Vapor Detection. *Nano Lett.* **2003**, *3*, 929−933.

(34) Yang, L.; Xiao, W.; Wang, J.; Li, X.; Wang, L. Tunable formaldehyde sensing properties of palladium cluster decorated graphene. *RSC Adv.* **2021**, *11*, 37120−37130.

(35) Gregersen, S. S.; Garcia, J. H.; Jauho, A.-P.; Roche, S.; Power, S. R. Charge and spin transport anisotropy in nanopatterned graphene. *J. Phys. Mater.* **2018**, *1*, 015005.

(36) Odaka, S.; Miyazaki, H.; Li, S.-L.; Kanda, A.; Morita, K.; Tanaka, S.; Miyata, Y.; Kataura, H.; Tsukagoshi, K.; Aoyagi, Y. Anisotropic transport in graphene on SiC substrate with periodic nanofacets. *Appl. Phys. Lett.* **2010**, *96*, 062111.